Chaos synchronization in coupled systems by applying pinning control

Meng Zhan,[1,*] Jihua Gao,[2] Ye Wu,[1,3,4] and Jinghua Xiao[4]
[1]*Wuhan Institute of Physics and Mathematics, Chinese Academy of Sciences, Wuhan 430071, China*
[2]*School of Materials, Shenzhen University, Shenzhen 518060, China*
[3]*Graduate School of the Chinese Academy of Science, Beijing 100049, China*
[4]*Department of Basic Science, Beijing University of Posts and Telecommunications, Beijing 100876, China*
(Received 9 September 2006; revised manuscript received 1 July 2007; published 10 September 2007)

Chaos synchronization in coupled chaotic oscillator systems with diffusive and gradient couplings forced by only one local feedback injection signal (boundary pinning control) is studied. By using eigenvalue analysis, we obtain controllable regions directly in control parameter space for different types of coupling links (including diagonal coupling and nondiagonal couplings). The effects of both diffusive and gradient couplings on chaos synchronization become clear. Some relevant factors on control efficiency such as coupled system size, transient process, and feedback signal intensity are also studied.

DOI: 10.1103/PhysRevE.76.036203 PACS number(s): 05.45.−a, 05.45.Xt

Since last decade the investigations of both control [1–17] and synchronization [18–24] in chaotic systems have attracted much attention in nonlinear dynamics field. For recent review papers on these subjects, see, e.g., Refs. [25], and references therein. Usually the objective of chaos control is to purposely achieve a desirable regular state (such as stationary or periodic motion) in an originally chaotic system. In contrast, chaos synchronization mostly focuses on self-organized synchronization behaviors in coupled chaotic systems. However, they are closely connected. Generally speaking, chaos synchronization can also be viewed as one special control if a chaotic target state is selected. The techniques and analysis methods independently developed in chaos control and chaos synchronization have quickly merged after the early stage of studying.

Recently due to both theoretical interests and practical applications, the research hot spot has shifted from the study of low-dimensional systems with finite low degrees of freedom to that of spatiotemporal chaotic systems characterized with much larger number of positive Lyapunov exponents. Several novel control techniques on spatiotemporal systems have been proposed so far, such as the local feedback (pinning) method [5–7], time-delay feedback method [8], feedback technique in Fourier space [9], phase space compression method [10], random itinerant feedback technique [11], and tailoring wavelets approach [12]. Among them, the pinning method by using local feedbacks has been extensively studied and tested in various systems, for example, coupled map lattices, coupled chaotic oscillators, partial differential equation systems, and so on [5–7,13–17]. On the other hand, in the study of chaos synchronization of coupled identical systems with the nearest diffusive coupling, Heagy *et al.* [19] well analyzed the stability of synchronous chaotic states by using the Fourier mode transform and the scaling transform among transverse modes directly in parameter space. In Ref. [24], one of us extended the above analysis to investigate the case with both the diffusive and gradient couplings. However, the diagonalization of the Jacobian via Fourier mode transform is only possible for the coupled system whose coupling configuration is shift invariant. Therefore, recently some new theories successfully dealing with the stability of synchronous chaotic states with various coupling configurations, such as the master stability function method [21] and the eigenvalue analysis method [22,23], have been developed, which solved, once and for all, the problem of synchronous stability for any linear coupling of chaotic oscillators. Both the above synchronization analysis approaches are represented in the space of $\mathrm{Re}(\lambda)$ and $\mathrm{Im}(\lambda)$, with λ being the eigenvalue of coupling matrix, and not explicitly shown in a control parameter space. For the sake of application, however, one always hopes to obtain a phase diagram explaining all different dynamical behaviors explicitly (or simply a controllability parameter region in our control problem). In the present work, by using the eigenvalue analysis method we generalize the pinning method developed in chaos control field to achieve synchronization in coupled chaotic oscillators. The controllability conditions with only one injection signal (boundary pinning control) for diagonal and nondiagonal couplings are theoretically analyzed, and some relevant problems on control efficiency are investigated.

We consider N coupled identical nonlinear oscillators with nearest couplings [24] under the first site being controlled,

$$\frac{du_j}{dt} = f(u_j) + \frac{\varepsilon - r}{2}\Gamma(u_{j+1} - u_j) + \frac{\varepsilon + r}{2}\Gamma(u_{j-1} - u_j) + c\Gamma[s(t) - u_j]\delta_{j,1}, \quad j = 1,2,\ldots,N, \tag{1}$$

where $u_j \in R^n$, the function f is nonlinear and capable of exhibiting chaotic solutions, ε and r are scalar diffusive and gradient coupling parameters, respectively, Γ denotes a $n \times n$ constant matrix linking coupled variables, the driving signal from a free oscillator $s(t)$ could conduct a chaotic motion $\{ds(t)/dt = f[s(t)]\}$, c indicates pinning strength, and $\delta_{j,1} = 1$ for $j = 1$ and $\delta_{j,1} = 0$ otherwise. Here periodic boundary conditions are adopted. With control, Eqs. (1) can be linearized around the target state $s(t)$, and we get the coupling matrix

*zhanmeng@wipm.ac.cn

$$A = \begin{pmatrix} -\varepsilon - c & \frac{\varepsilon - r}{2} & 0 & \cdots & \frac{\varepsilon + r}{2} \\ \frac{\varepsilon + r}{2} & -\varepsilon & \frac{\varepsilon - r}{2} & \cdots & 0 \\ \vdots & \vdots & \ddots & \cdots & \cdots \\ \vdots & \vdots & \vdots & \ddots & \frac{\varepsilon - r}{2} \\ \frac{\varepsilon - r}{2} & 0 & \cdots & \frac{\varepsilon + r}{2} & -\varepsilon \end{pmatrix}_{N \times N}. \quad (2)$$

Before our model study, we should emphasize that, in Ref. [24], by using the Fourier mode transform and the scaling relationship one of us has intensively studied the chaos synchronization problem of the free systems without the control term in Eqs. (1), and successfully answered the question: under what coupling strength conditions can we observe the synchronization in the free systems? In that work the stability boundaries of all transverse modes are simultaneously drawn by justifying the boundary of a single mode with a scaling relation, and we obtain the stable synchronization regions explicitly in the control parameter space from the overlap of the stable regions of all transverse modes. In contrast, in the present work, we intend to study the control problem and want to solve a different question: under what coupling conditions can we accomplish chaos synchronization in the coupled systems if we switch on our control term in Eqs. (1)? These two works are closely connected, however, both the objectives and the analytical methods are distinct, as we will see below.

As now one oscillator is pinned, the translational invariance is immediately broken and the usual Fourier transform method utilized in Refs. [19,24] is not workable. We have to rely on more general method, for example, the eigenvalue analysis. The essential idea of the eigenvalue analysis approach proposed in Refs. [22,23] is to separate the complicated stability problem of Eqs. (1) (or any linearly coupled systems) into two independent problems: one is to analyze the stable regions of one single mode equation

$$\frac{d\eta}{dt} = (Df(s) - [\mathrm{Re}(\lambda) + i\,\mathrm{Im}(\lambda)]\Gamma)\,\eta, \quad (3)$$

which depends on the single-site parameters only [such as the reference orbit $s(t)$, the Jacobian $Df(s)$, and the inner linking matrix Γ]; the other is to analyze the eigenvalue distribution of the linear coupling matrix A, which depends on the coupling parameters, ε and r, the driving parameter c, and the system size N only, and is independent of the inner dynamics. The key point for the synchronous state to be stable is that all eigenvalues of the matrix A except the one with $\lambda = 0$ (corresponding to the spatially homogeneous state) are well located in the stable region in Eq. (3). The stable region surrounded by the so-called critical curve can be numerically obtained. The eigenvalue distribution can also be numerically calculated or theoretically analyzed for some special cases, such as the matrix A or B in controlled system studied below. Thus, the problem of the synchronous stability has been well solved. For more details, see Refs. [22,23]. For convenience, we put a minus sign in front of the λ in Eq. (3). Obviously, this more general approach can easily solve chaotic synchronization in coupled identical systems with nearest coupling, which has been studied by Heagy *et al.* [19] with the Fourier mode transform method.

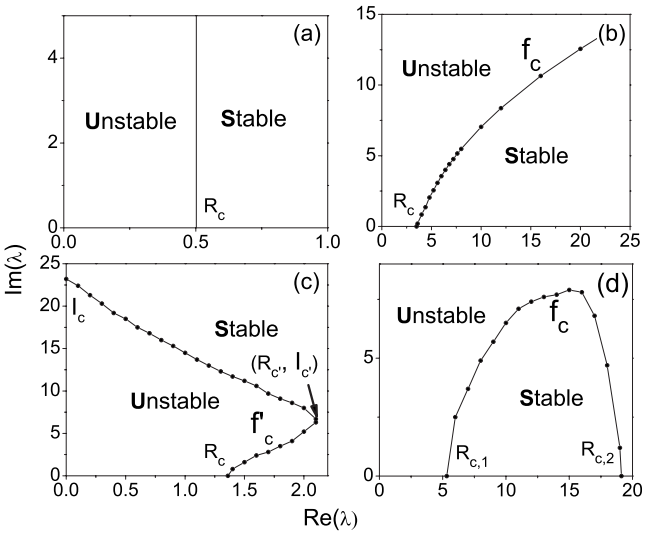

FIG. 1. The four types of critical curves for (a) diagonal coupling, (b) type I, (c) type II, and (d) type III nondiagonal couplings.

(a) $\Gamma = \begin{pmatrix} 1 & 0 & 0 \\ 0 & 1 & 0 \\ 0 & 0 & 1 \end{pmatrix}$, (b) $\Gamma = \begin{pmatrix} 0 & 0 & 0 \\ 1 & 0 & 0 \\ 0 & 0 & 0 \end{pmatrix}$, (c) $\Gamma = \begin{pmatrix} 0 & 0 & 0 \\ 0 & 1 & 0 \\ 0 & 0 & 0 \end{pmatrix}$,

and (d) $\Gamma = \begin{pmatrix} 0 & 1 & 0 \\ 0 & 0 & 0 \\ 0 & 0 & 0 \end{pmatrix}$.

As an example, without losing generality, the model of coupled Lorenz oscillators has been chosen, in which the single system reads $\dot{x}_1 = \sigma(x_2 - x_1)$, $\dot{x}_2 = \rho x_1 - x_2 - x_1 x_3$, $\dot{x}_3 = x_1 x_2 - \beta x_3$. $\sigma = 10.0$, $\beta = 1.0$, and $\rho = 28.0$; at these parameters the system is chaotic, which is characterized by a positive largest Lyapunov exponent $\lambda_0 \approx 0.502 > 0$. Here we have chosen the same model and parameter setting as Ref. [24]. In Figs. 1(a)–1(d), we plot the critical boundaries in the $\mathrm{Re}(\lambda) - \mathrm{Im}(\lambda)$ parameter space for different coupling links Γ's by using the results in our previous paper [24] and applying a simple scaling transformation to both the abscissa and the ordinate. Figures 1(a)–1(d) correspond to four types of critical curves of the diagonal coupling, the nondiagonal types I, II, and III couplings for the linking matrices

$$\Gamma = \begin{pmatrix} 1 & 0 & 0 \\ 0 & 1 & 0 \\ 0 & 0 & 1 \end{pmatrix}, \quad \begin{pmatrix} 0 & 0 & 0 \\ 1 & 0 & 0 \\ 0 & 0 & 0 \end{pmatrix}, \quad \begin{pmatrix} 0 & 0 & 0 \\ 0 & 1 & 0 \\ 0 & 0 & 0 \end{pmatrix},$$

and $\begin{pmatrix} 0 & 1 & 0 \\ 0 & 0 & 0 \\ 0 & 0 & 0 \end{pmatrix}$,

respectively. We use f_c to represent critical curve ($\mathrm{Im}(\lambda) = f_c[\mathrm{Re}(\lambda)]$). The critical curves are obtained by the compu-

tation of the largest Lyapunov exponent of the linearization equation [Eq. (3)]; the numerical method is similar to the classical algorithm of the largest Lyapunov exponent for single nonlinear system used in Ref. [26], except that now the impacts of Re(λ) and Im(λ) have to be considered. For the case of the diagonal coupling, the stability is controlled by the value of Re(λ) only [not Im(λ)], and the threshold value of the stable-unstable boundary at the real axis $R_c = \lambda_0 = 0.502$.

For an extreme case [an infinitely strong driving ($c \to +\infty$)], the $N \times N$ matrix A given above should be changed to

$$B = \begin{pmatrix} -\varepsilon & \frac{\varepsilon - r}{2} & 0 & \cdots & 0 \\ \frac{\varepsilon + r}{2} & -\varepsilon & \frac{\varepsilon - r}{2} & \cdots & 0 \\ \vdots & \vdots & \ddots & \cdots & \cdots \\ \vdots & \vdots & \vdots & \ddots & \frac{\varepsilon - r}{2} \\ 0 & 0 & \cdots & \frac{\varepsilon + r}{2} & -\varepsilon \end{pmatrix}_{(N-1)\times(N-1)} \tag{4}$$

after we remove both the first row and the first column. The physical meaning is straightforward: As the first oscillator can be surely pinned to the target state for $c \to +\infty$, we only need to pay attention to the stability of the remaining $N-1$ oscillators. A rigorous mathematical proof can be found in Lemma 1.2 in Ref. [27]. The $N-1$ eigenvalues of $-B$ can be explicitly given [28]

$$\lambda_j = \varepsilon - \sqrt{\varepsilon^2 - r^2} \cos \frac{j\pi}{N}, \quad j = 1,2, \ldots, N-1 \tag{5}$$

which has also been derived in different circumstances [3,7]. In Ref. [7], in order to control the system to a homogeneous stationary state, the eigenvalue distribution of Eq. (5) has been used to schematically show the control efficiency. The above eigenvalue spectrum is substantially different from that of the coupling circular matrix for the free systems, which has been explicitly given in Eq. (2b) in Ref. [24]. However, the geometrical structure of the eigenvalue distribution of $-B$ is also simple. If $\varepsilon \geq r$, $\mathrm{Im}(\lambda_j) = 0$ and $\lambda_j = \mathrm{Re}(\lambda_j) = \varepsilon - \sqrt{\varepsilon^2 - r^2} \cos \frac{j\pi}{N}$; all eigenvalues are real and they are located exactly on the real axis as one horizontal line from $x = \varepsilon - \sqrt{\varepsilon^2 - r^2} \cos \frac{\pi}{N}$ (the leftmost point) to $x = \varepsilon + \sqrt{\varepsilon^2 - r^2} \cos \frac{\pi}{N}$ (the rightmost one). Whereas if $\varepsilon < r$, $\mathrm{Re}(\lambda_j) = \varepsilon$ and $\mathrm{Im}(\lambda_j) = \sqrt{r^2 - \varepsilon^2} \cos \frac{j\pi}{N}$; all eigenvalues are complex and they stay at $x = \varepsilon$ as one vertical line from $y = -\sqrt{r^2 - \varepsilon^2} \cos \frac{\pi}{N}$ (the lowest point) to $y = \sqrt{r^2 - \varepsilon^2} \cos \frac{\pi}{N}$ (the uppermost one). Therefore, by the demand that all eigenvalues of linking matrices get into stable domains of diagrams in Fig. 1, what we need to do next is to analyze the eigenvalue distribution with the above simple geometrical structure (one horizontal line for $\varepsilon \geq r$ and one vertical line for $\varepsilon < r$) and consider the restriction of different critical curves

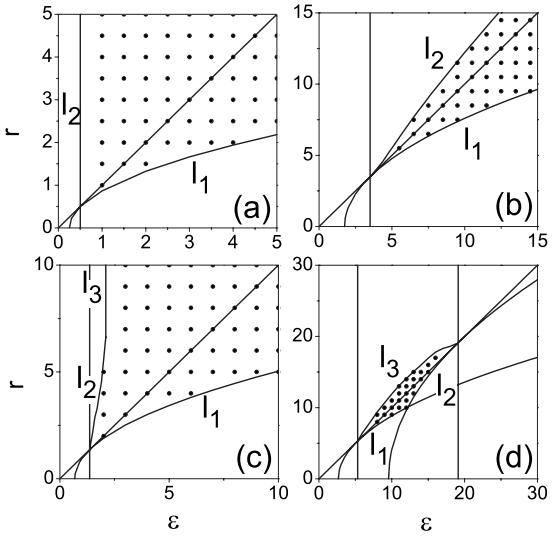

FIG. 2. The controllable regions in the ε-r parameter space for different Γ's. Both the system size N and the driving force c are infinite. The positions of the curves l_1, l_2, and l_3 are analytically obtained.

for different coupling matrices. Note, the eigenvalue distribution of the coupling $-B$ is independent of different Γ's.

First, let us consider an infinite array ($N \to +\infty$, $\cos \frac{\pi}{N} \to 1$); the extension to finite number is straightforward and will be studied below. For the diagonal matrix in Fig. 1(a), if $\varepsilon \geq r$, the necessary condition for stable synchronization is that the smallest eigenvalue λ_1 ($\lambda_1 \simeq \varepsilon - \sqrt{\varepsilon^2 - r^2}$) is larger than or equal to R_c. $R_c = 0.502$. Directly we have

$$\varepsilon \geq r \geq \sqrt{R_c(2\varepsilon - R_c)}. \tag{6}$$

If $\varepsilon < r$, for this simplest case, all eigenvalues should locate at the right-hand of the vertical straight line $x = R_c$. We get another inequality

$$r > \varepsilon \geq R_c. \tag{7}$$

Thus, in the ε-r space we obtain the controllability parameter region, which is surrounded by the two curves: $r = \sqrt{R_c(2\varepsilon - R_c)}$ (curve l_1) and $\varepsilon = R_c$ (line l_2) [Fig. 2(a)].

We can apply the above idea to other more complicated cases. For nondiagonal type-I link [Fig. 1(b)], if $\varepsilon < r$, the synchronous state becomes unstable after λ_1 and λ_{N-1} go across the critical curve f_c at the same time; correspondingly we have $\sqrt{r^2 - \varepsilon^2} \leq f_c(\varepsilon)$ and, further,

$$\sqrt{f_c^2(\varepsilon) + \varepsilon^2} \geq r > \varepsilon. \tag{8}$$

As a result, the field surrounded by the two functions: $r = \sqrt{R_c(2\varepsilon - R_c)}$ (curve l_1) and $r = \sqrt{f_c^2(\varepsilon) + \varepsilon^2}$ (curve l_2) constitutes the controllable region [Fig. 2(b)]. $R_c = 3.5$.

For type-II critical curve [1(c)], it has to be separately considered for $y \leq I_{c'}$ and $I_{c'} < y \leq I_c$. $(R_{c'}, I_{c'})$ is the changing point, as indicated by an arrow in Fig. 1(c). If $\varepsilon < r$ and $\varepsilon \geq R_{c'}$, the synchronous chaos state is always stable; this situation is analogous to the diagonal coupling. Whereas if $\varepsilon < r$ and $R_{c'} > \varepsilon > R_c$, it gets unstable after the two eigen-

values, λ_1 and λ_{N-1}, move across the lower branch of the critical curve f_c' at $R_{c'} > x > R_c$; this case is similar to the above type-I link. Hence the controllability parameter region is constructed by the three functions $r=\sqrt{R_c(2\varepsilon - R_c)}$ (curve l_1), $r=\sqrt{f_c'^2(\varepsilon)+\varepsilon^2}$ for $R_{c'} > \varepsilon > R_c$ (curve l_2), and $\varepsilon = R_{c'}$ for $r \geq I_{c'}$ (line l_3), as illustrated in Fig. 2(c). $R_c=1.36$, $I_c=23.2$, $R_{c'}=2.1$, and $I_{c'}=6.6$.

For the last case, type-III [(d)], the second threshold $R_{c,2}$ has to be considered. If $\varepsilon > r$, we should put all $N-1$ eigenvalues into the stable region $(R_{c,1}, R_{c,2})$, and we have $\varepsilon - \sqrt{\varepsilon^2 - r^2} \geq R_{c,1}$ and $\varepsilon + \sqrt{\varepsilon^2 - r^2} \leq R_{c,2}$ or, equivalently,

$$r \geq \sqrt{R_{c,1}(2\varepsilon - R_{c,1})} \tag{9}$$

and

$$r \geq \sqrt{R_{c,2}(2\varepsilon - R_{c,2})}. \tag{10}$$

As a consequence, we obtain the controllability parameter region explicitly encircled by the three curves [Fig. 2(d)]: $r = \sqrt{R_{c,1}(2\varepsilon - R_{c,1})}$ (curve l_1), $r=\sqrt{R_{c,2}(2\varepsilon - R_{c,2})}$ (curve l_2), and $r=\sqrt{f_c^2(\varepsilon)+\varepsilon^2}$ (curve l_3). $R_{c,1}=5.32$ and $R_{c,2}=19.12$.

In Figs. 2(a)–2(d), we predict the controllable regions for different Γ's by applying the above analyses. The theoretical results are in good agreement with our numerical simulations, indicated by the dotted regions, and now the controllability conditions become clear. First, we may ask can we realize control (or synchronization) by using only one injection feedback into such infinitely large systems ($N \to +\infty$) by varying the diffusive and gradient couplings ε and r? The answer is yes. More specifically, for the diagonal coupling [Figs. 1(a) and 2(a)], we can do so by increasing the gradient coupling r; for type II nondiagonal coupling [Figs. 1(c) and 2(c)], we can also do so after the diffusive coupling ε is larger than a critical value ($\varepsilon \geq R_{c'}$); for type I coupling [Figs. 1(b) and 2(b)], it is again correct for intermediate values of ε and r around $\varepsilon \approx r$, and it is unavailable for either larger or smaller ε (r) with fixed r (ε); and for type III [Figs. 1(d) and 2(d)], quite different from other cases, it is possible only under finite coupling strengths of both ε and r; in this case, the parameter region is a close set.

Second, there are some common features for all couplings. It is valuable to briefly analyze the geometrical structure for the two major critical curves $r=f_1(\varepsilon)=\sqrt{R_c(2\varepsilon - R_c)}$ and $r=f_2(\varepsilon)=\sqrt{f_c^2(\varepsilon)+\varepsilon^2}$. As $f_1(R_c/2)=0$, $f_1(R_c)=R_c$, $\frac{df_1(\varepsilon)}{d\varepsilon}|_{\varepsilon=R_c}=1$, $\frac{df_1(\varepsilon)}{d\varepsilon}|_{\varepsilon\to\infty}=0$, and $\frac{df_1(\varepsilon)}{d\varepsilon} > 0$ for $\varepsilon > \frac{R_c}{2}$, the curve f_1 starts from point $(R_c/2, 0)$, monotonically increases, and intersects tangentially with the diagonal at $r=\varepsilon=R_c$; f_2 also intersects with the diagonal at point (R_c, R_c), since $f_2(R_c) = R_c$. Consequently in Fig. 2 all the controllable regions start from one critical parameter point (R_c, R_c), and the spaces are blank for either ε or r being smaller than R_c. Note, R_c can be different for different couplings. Thus we know that both ε and r play constructive roles in chaos controllability, and sole coupling without the opposite one [ε (or r) alone] is not sufficient for the observation of successful control, which is only possible for $\varepsilon \geq R_c$ and $r \geq R_c$ instead.

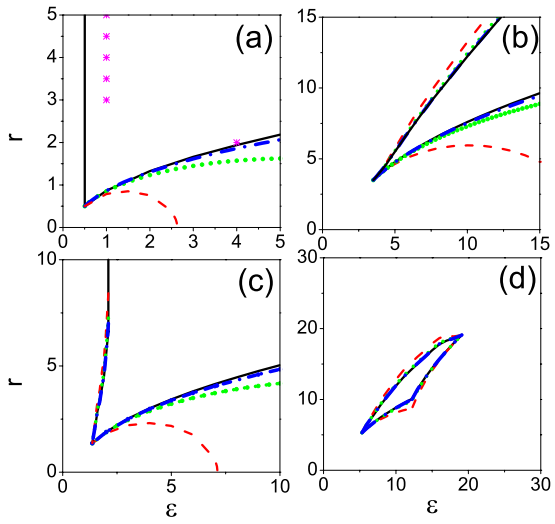

FIG. 3. (Color online) The same as Fig. 2 for finite system sizes N. N is 5 (dashed line), 10 (dotted line), 20 (dash-dotted line), and infinity (solid line), respectively. In (a), under the parameters indicated by stars, the transient time increases exponentially with the system size. While at other parameters within the controllable region, linear increasing is observed.

Third, for the extreme situation ($\varepsilon = r$), the bidirectionally coupled system with the periodic boundary [Eqs. (1)] degenerates to a one-way coupled system, where the control problem has been extensively studied recently [3,4,6,7]. Some of us discovered that the existence of gradient force is of crucial importance for enhancing the control efficiency [6,7]. One might intuitively believe that the stronger the force, the better it is. From the knowledge in Fig. 2(d) for type III link, however, we know this is not always the case and sufficiently large one-way coupling sometimes may even break control. Note, most existing studies have chosen one-way coupled lattice maps as model (usually logistic map, which has only one variable), where non-diagonal coupling is impossible.

Next we clarify the effect of finite system size N by considering the $\cos\frac{\pi}{N}$ term in Eq. (5) for different Γ's. In Fig. 3, we plot the controllability parameter regions for N being 5 (dashed line), 10 (dotted line), 20 (dash-dotted line), and infinity (solid line), respectively. Apparently, the larger N, the smaller synchronization region we get; as N is moderately large (for instance, $N=20$, $\cos\frac{\pi}{N}=0.988 \approx 1$), the region gets undistinguished with that for infinite N.

From practical applications point of view, it is very important to study transient process. Much short transient is preferred and believed as a high control efficiency. The evolution process, shown in Fig. 4(a) for diagonal coupling, $\varepsilon = 2$ and $r=4$, where successful control is achieved at very short time $t \approx 20$, tells us the control efficiency with the current boundary pinning method is really very high. The underlying mechanism with the synchronization cascade propagation from j to $j+1$ and subsequently extension to the whole array has been discovered [Fig. 4(a)]. Therefore, a linear increase of the average transient time versus the system size is expected, which has been well confirmed in

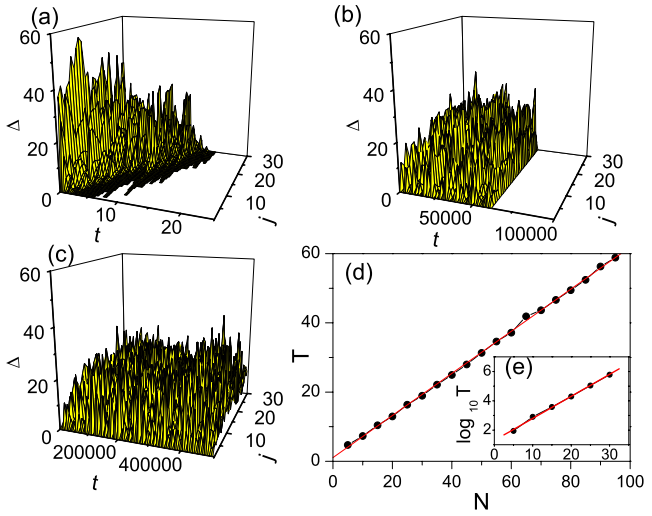

FIG. 4. (Color online) (a)–(c) The time evolution of the variable difference Δ under different parameter sets (a) $\varepsilon=2$, $r=4$, (b) $\varepsilon=1$, $r=4$, and (c) $\varepsilon=0.5$, $r=4$. $\Delta_j(t)=\sqrt{(x_j-x_1)^2+(y_j-y_1)^2+(z_j-z_1)^2}$. $N=30$. (d), (e) The linear and exponential dependencies of the transient time T vs the system size N for (d) $\varepsilon=2$, $r=4$ and (e) $\varepsilon=1$, $r=4$.

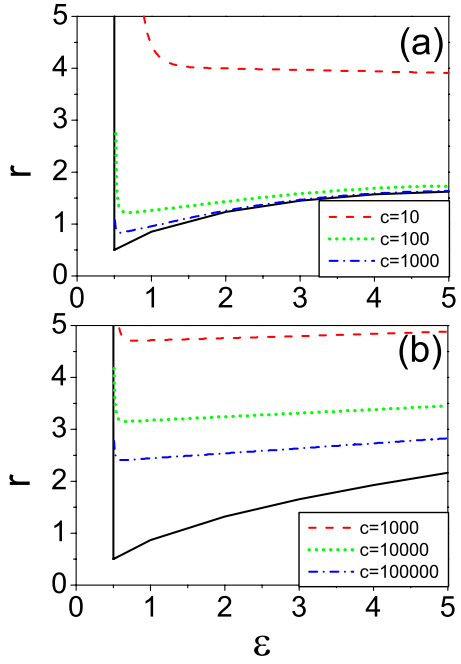

FIG. 5. (Color online) The controllable regions (above the lines) for diagonal coupling for both finite system size N and finite driving strength c. (a) $N=10$; from upper to lower, $c=10$ (dashed), 100 (dotted), 1000 (dash-dotted), and infinity (solid line), respectively. (b) $N=50$; from upper to lower, $c=1000$ (dashed), 10000 (dotted), 100 000 (dash-dotted), and infinity (solid line), respectively.

Fig. 4(d). Clearly this characteristic is extremely useful for applications. However, at some parameters close to the critical curves [indicated with stars in Fig. 3(a)], e.g., $\varepsilon=1$ and $r=4$, we also find another kind of transient behavior that all coupled oscillators transit to chaotic synchronization simultaneously with an extremely long transient time ($t\approx 61000$) [Fig. 4(b)] and an exponential dependence of T on N [Fig. 4(e)]. This case might be similar to the usual transient chaos process around critical control parameter. For comparison, we plot the case for $\varepsilon=0.5$ and $r=4$ ($\varepsilon\lesssim R_c=0.502$) in Fig. 4(c), where synchronization is unavailable. Therefore, from the above numerical results we know that if it is possible, in applications we should purposely choose parameters around $\varepsilon=r$ (far away the critical curves as possible) to short waiting time and achieve high efficiency.

In the end, the situation for finite driving strength c is briefly explored in Fig. 5. Although now we cannot get the explicit expression of the eigenvalue spectrum from the coupling matrix $-A$ as Eq. (5), the eigenvalue analysis method is still applicable. For the simplest case (the diagonal coupling), we numerically compute the N eigenvalues λ_j, analyze the distribution for different (ε,r) in the $\mathrm{Re}(\lambda)-\mathrm{Im}(\lambda)$ space, and show the results in Fig. 5 for different N and c [$N=10$ and 50 in Figs. 5(a) and 5(b), respectively]. Above these lines, synchronization is stable. Apparently a larger driving c is needed for larger N; this consists with our heuristic understanding.

In conclusion, we have studied chaos synchronization in coupled chaotic oscillators with both diffusive and gradient couplings by using the chaos control technique (pinning method) and the eigenvalue analysis method. It is the first time to study in detail the pinning control problem with nondiagonal couplings and obtain controllability parameter regions explicitly in control parameter space for all different types of critical curves of the coupling links, whose classification seems to have been exhausted, to the best of our knowledge. Some remarkable findings are both diffusive and gradient couplings are of significant importance for successful control, the system with individual coupling (zero diffusive coupling or zero gradient coupling) is uncontrollable with the present pinning method, and larger one-way coupling strength with equal diffusive and gradient couplings may even break stable synchronous state for type-III curve. Although we have used the numerical results (characteristic critical curves for nondiagonal links) directly from our previous paper on coupled Lorenz oscillators in free system [24], it is simply for convenience, and the analytical method and the theoretical results presented in this paper could be applicable to other systems easily. Some more comparisons with the results in Ref. [24], where the trivial case with diagonal link was not discussed, are interesting. There, for nondiagonal type III coupling, chaos synchronization is unavailable for the system size being larger than 5; for type I and type II couplings, much larger intensities for both the diffusive and gradient couplings are needed as the system size N increases. Therefore, in free system, in fact we cannot realize chaos synchronization for sufficiently large system, let alone infinite N. In sharp contrast with this point, stable homogeneous chaotic synchronization in the extremely large systems (infinite N) has been quickly reached after we substitute only one site with the external forcing signal (infinite c), and the boundary pinning control has been demonstrated

to be highly successful for all links (Fig. 2) with strikingly high control efficiency (Fig. 4).

This work was partially supported by the Foundation of Wuhan Institute of Physics and Mathematics under Grant No. T06S607, and the National Natural Science Foundation of China under Grant No. 10675161. The work of J.G. was supported by the National Natural Science Foundation of China under Grant No. 10405018. We thank the anonymous referees for criticisms.

[1] E. Ott, C. Grebogi, and J. A. Yorke, Phys. Rev. Lett. **64**, 1196 (1990).
[2] K. Pyragas, Phys. Lett. A **170**, 421 (1992).
[3] I. Aranson, D. Golomb, and H. Sompolinsky, Phys. Rev. Lett. **68**, 3495 (1992).
[4] D. Auerbach, Phys. Rev. Lett. **72**, 1184 (1994).
[5] Hu Gang and Qu Zhilin, Phys. Rev. Lett. **72**, 68 (1994).
[6] J. H. Xiao, G. Hu, J. Z. Yang, and J. H. Gao, Phys. Rev. Lett. **81**, 5552 (1998).
[7] Hu Gang, X. Jinghua, G. Jihua, Li Xiangming, Y. Yugui, and B. Hu, Phys. Rev. E **62**, R3043 (2000).
[8] M. E. Bleich and J. E. S. Socolar, Phys. Rev. E **54**, R17 (1996).
[9] G. K. Harkness, R. Martin, A. J. Scroggie, G.-L. Oppo, and W. J. Firth, Phys. Rev. A **58**, 2577 (1998).
[10] X. Zhang and K. Shen, Phys. Rev. E **63**, 046212 (2001).
[11] J. H. Gao, X. G. Wang, G. Hu, and J. H. Xiao, Phys. Lett. A **283**, 342 (2001).
[12] G. W. Wei, M. Zhan, and C.-H. Lai, Phys. Rev. Lett. **89**, 284103 (2002).
[13] Y. S. Kwon, S. W. Ham, and K. K. Lee, Phys. Rev. E **55**, 2009 (1997).
[14] R. O. Grigoriev, M. C. Cross, and H. G. Schuster, Phys. Rev. Lett. **79**, 2795 (1997).
[15] Y. C. Kouomou and P. Woafo, Phys. Rev. E **66**, 066201 (2002).
[16] G. Greilich, M. Markus, and E. Goles, Eur. Phys. J. D **33**, 279 (2005).
[17] S. G. Guan, Y. C. Zhou, G. W. Wei, and C.-H. Lai, Chaos **13**, 64 (2003).
[18] L. M. Pecora and T. L. Carroll, Phys. Rev. Lett. **64**, 821 (1990).
[19] J. F. Heagy, L. M. Pecora, and T. L. Carroll, Phys. Rev. Lett. **74**, 4185 (1995).
[20] L. M. Pecora, T. L. Carroll, G. A. Johnson, D. J. Mar, and J. F. Heagy, Chaos **7**, 520 (1997).
[21] L. M. Pecora and T. L. Carroll, Phys. Rev. Lett. **80**, 2109 (1998).
[22] J. Z. Yang, G. Hu, and J. H. Xiao, Phys. Rev. Lett. **80**, 496 (1998).
[23] G. Hu, J. Z. Yang, and W. J. Liu, Phys. Rev. E **58**, 4440 (1998).
[24] M. Zhan, G. Hu, and J. Z. Yang, Phys. Rev. E **62**, 2963 (2000).
[25] S. Boccaletti, C. Grebogi, Y. C. Lai, H. Mancini, and D. Maza, Phys. Rep. **329**, 103 (2000); S. Boccaletti, J. Kurths, G. Osipov, D. L. Valladares, and C. S. Zhou, *ibid.* **366**, 1 (2002); Chaos **13**, 1 (2003).
[26] A. Wolf, J. B. Swift, H. L. Swinney, and J. A. Vastano, Physica D **16**, 285 (1985).
[27] L. Caffarelli, L. Nirenberg, and J. Spruck, Acta Math. **155**, 261 (1985).
[28] G. Strang, *Linear Algebra and its Applications* (Academic Press, London, 1976); I. V. Proskuryakov, *Problems in Linear Algebra* (Mir Publishers, Moscow, 1985).